ADVANCED FUNCTIONAL MATERIALS
www.afm-journal.de

Materials Views
www.MaterialsViews.com

High-Density Hotspots Engineered by Naturally Piled-Up Subwavelength Structures in Three-Dimensional Copper Butterfly Wing Scales for Surface-Enhanced Raman Scattering Detection

Yongwen Tan, Jiajun Gu, Linhua Xu, Xining Zang, Dingxin Liu, Wang Zhang, Qinglei Liu, Shenmin Zhu, Huilan Su, Chuanliang Feng, Genlian Fan, and Di Zhang**

Very recently, wing scales of natural *Lepidopterans* (butterflies and moths) manifested themselves in providing excellent three dimensional (3D) hierarchical structures for surface-enhanced Raman scattering (SERS) detection. But the origin of the observed enormous Raman enhancement of the analytes on 3D metallic replicas of butterfly wing scales has not been clarified yet, hindering a full utilization of this huge natural wealth with more than 175 000 3D morphologies. Herein, the 3D sub-micrometer Cu structures replicated from butterfly wing scales are successfully tuned by modifying the Cu deposition time. An optimized Cu plating process (10 min in Cu deposition) yields replicas with the best conformal morphologies of original wing scales and in turn the best SERS performance. Simulation results show that the so-called "rib-structures" in Cu butterfly wing scales present naturally piled-up hotspots where electromagnetic fields are substantially amplified, giving rise to a much higher hotspot density than in plain 2D Cu structures. Such a mechanism is further verified in several Cu replicas of scales from various butterfly species. This finding paves the way to the optimal scale candidates out of ca. 175 000 *Lepidopteran* species as bio-templates to replicate for SERS applications, and thus helps bring affordable SERS substrates as consumables with high sensitivity, high reproducibility, and low cost to ordinary laboratories across the world.

1. Introduction

Developing metallic substrates based on surface-enhanced Raman scattering (SERS) phenomenon has recently become one of the most exciting interdisciplinary research areas owing to its broad applications in trace-amount chemical analyses.[1–8] Recent works have provided excellent SERS substrates based on sub-micrometer metallic structures, which were mainly created either by forming plasmonic nanoparticles (NPs) with special shapes and core-shell structures,[9–12] or by performing lithographic approaches, to chase high density "hotspots" where electromagnetic (EM) fields are localized.[13–16] Compared with two dimensional counterparts, three dimensional (3D) sub-micrometer structures have the potential to further expand the arrangement of hotspots along the third dimension, which could in turn increase the hotspot density.[17–20] However, it is quite difficult to conveniently generate reproducible 3D sub-micrometer structures with such hotspots at a low cost for research and for commercial applications. Very recently, we demonstrated that a direct replication of hierarchical 3D sub-micrometer structures of butterfly wing scales in metals yields excellent SERS substrates in terms of high sensitivity (one order of magnitude higher than Klarite, the most popular commercial SERS substrates to date, Renishaw Diagnostics), high reproductivity (comparable to the commercial counterparts), and low cost (ten times of magnitude cheaper than Klarite that is ca. $35 per piece as a consumable).[21] Since there are far more than 175 000 kinds of nature-designed 3D morphologies of butterfly scales, these novel materials provide promising solutions for substantially applicable SERS substrates, by which the research in a broad range of related fields might be lifted to a new level. Nevertheless, the origin of such gigantic Raman signal enhancement has still not been clarified yet,[22,23] hindering a full utilization of this huge natural wealth with more than 175 000 3D morphologies. Herein, we present a mechanism through which the 3D sub-micrometer copper structures with the morphologies inherited from natural butterfly wing scales can efficiently enhance the SERS properties. We tuned the morphologies of these "Cu butterfly wing scales" by changing the Cu deposition time, and found that the so called "rib-structures" with a period about 20–30 nm on the sidewalls of "main ridges" of scales

Dr. Y. W. Tan, Prof. J.-J. Gu, Mr. L. H. Xu, Ms. X. N. Zang, Dr. D. X. Liu, Dr. W. Zhang, Dr. Q. L. Liu, Prof. S. M. Zhu, Prof. H. L. Su, Prof. C. L. Feng, Dr. G. L. Fan, Prof. D. Zhang
State Key Laboratory of Metal Matrix Composites
Shanghai Jiao Tong University
800 Dongchuan Road, Shanghai 200240, P. R. China
E-mail: gujiajun@sjtu.edu.cn; zhangdi@sjtu.edu.cn

DOI: 10.1002/adfm.201102948

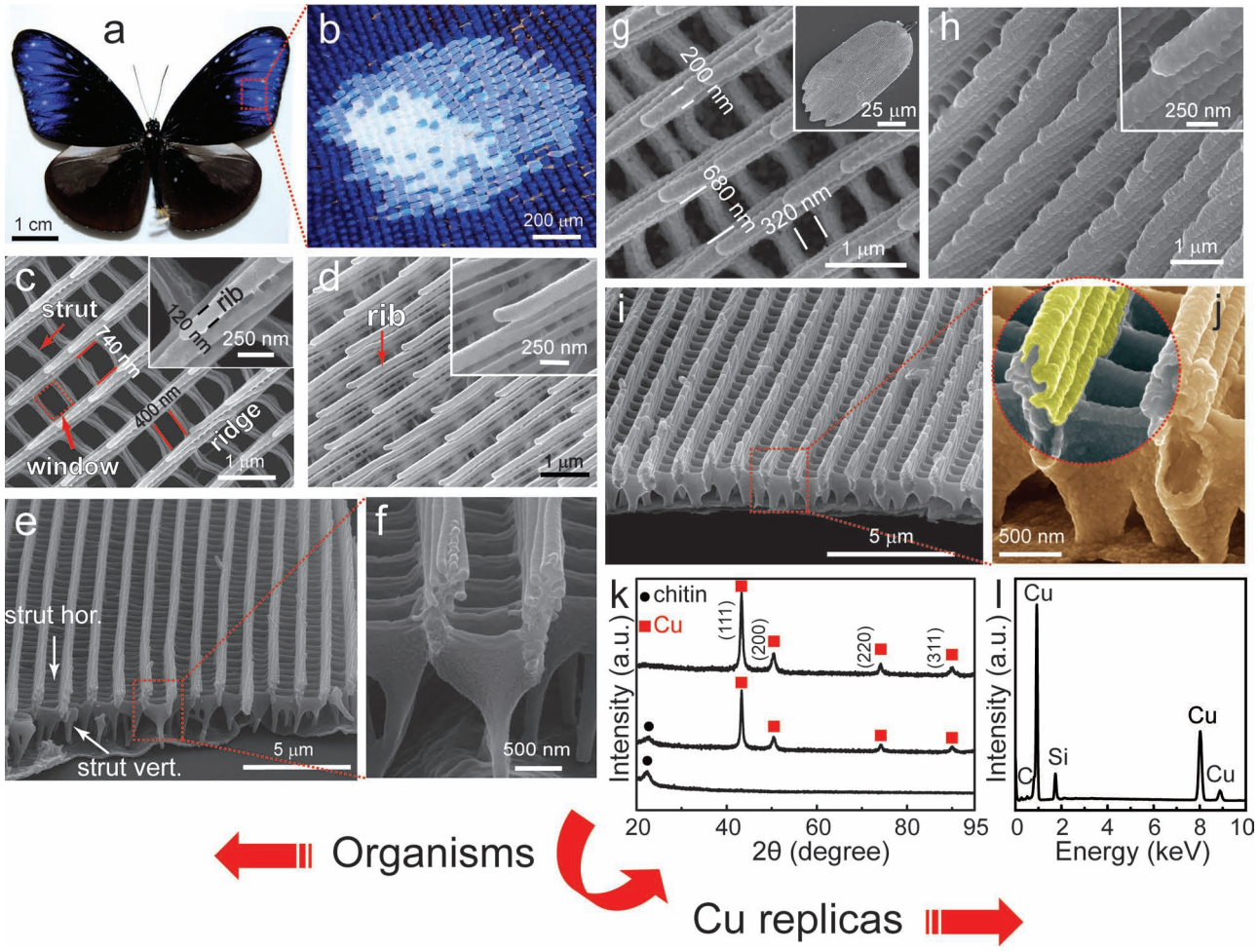

Figure 1. Morphologies of original butterfly wing scales and their Cu replicas on silicon wafers. a) *E. mulciber*. b) Optical microscope image of wing scales. c) Top view and d) side view of natural blue scales in b). Insets are FESEM images with a higher magnification. e) and f) Cross-section of scales. Definitions of various structural features and corresponding periodicities are marked in c)–e). g)–j) FESEM images of Cu scales obtained via electroless Cu deposition for 10 min. Note that all the Cu replicas in this work were imaged under high vacuum without any metal sputtering. The cross-section image i) of Cu scale shows that even vertical struts beneath the ridges were also conformally replicated, indicating that the uniform Cu deposition was achieved for interior structures as well. A close-up view j) suggests that the replicas were hollow, resulted from the removal of original chitin-based structures by H_3PO_4. Note the highlighted part in j) that reveals the "rib-structures" in Cu replicas. k) XRD results. Data from bottom to top were from original chitinous wings, Cu/wing-scale complexes, and Cu replicas, respectively. l) EDS results of the Cu replicas. Si signals originated from the Si wafers.

played a key role in piling hotspots up along the third dimension perpendicular to the scale surface. Our results help clarify the mechanism of the Raman enhancement originating from these natural gifts with 3D sub-micrometer structures, which are too complicated to design manually at present.

2. Results and Discussion

2.1. "Rib-Structures" in Cu Butterfly Wing Scales

Figure 1 demonstrates the dorsal forewing scales from *Euploea mulciber*, a butterfly species living in Southeast of Asia. The dorsal surface of an *E. mulciber* wing has a prominent shining metallic blue area decorated with some small white spots (Figure 1a), bearing hundreds of thousands of flat tiny chitin-based scales arranged in rows (Figure 1b). Figure 1c–f present the field-emission scanning electron microscopy (FESEM) images of 3D periodic sub-micrometer structures of its blue wing scales. Like many other *Lepidopterans* (butterflies and moths), the wing scale microstructures of *E. mulciber* include so-called "main ridges", horizontal and vertical "struts", and "ribs", et al., as marked in details in Figure 1c–e.[21,24,25]

Figure 1g–j show the FESEM images of as-synthesized Cu scale replicas experienced an electroless Cu plating for 10 min followed by exposure to H_3PO_4 to remove the original organisms. A general chemical synthesis route can be found in our previous work.[21] Lower magnification image (inset of Figure 1g) indicates that the whole single scale was perfectly preserved after the chemical treatments, owing to a homogeneous deposition of

Cu nanoparticles (NPs) across the whole scale. Higher magnification image shows that Cu NP layer conformally replicated the natural organisms down to a sub-micrometer level (further confirmed via transmission electron microscopy (TEM) observation in the Supporting Information, Figure S1), promising the formation of Cu plasmonic structures for subsequent SERS studies. It should be noted that not only the sub-micrometer-scaled parallel "main ridges", but also the nanometer-scaled "ribs" (overlapping layers within the ridges, see Figure 1j) were well inherited in the Cu replicas. To a natural butterfly, these structures are essential to the colorization of its wing scales for mating[26,27] and camouflage,[28,29] etc..

As shown by X-ray diffraction (XRD) results (Figure 1k), chitin-based wing organisms could be identified before the H_3PO_4 exposure, which disappeared after the removal of original bio-templates by H_3PO_4. After the electroless deposition of Cu NPs, face-centered-cubic (*fcc*) Cu with main diffraction peaks of {111}, {200}, {220}, and {311} could be indexed, with an average grain size of ca. 16.9 nm (Scherrer Formula). Figure 1l provides energy-dispersive X-ray spectrometry (EDS) results of Cu replicas, proving the successful replication in composition as well.[21]

To tell which structural feature as mentioned above plays a dominant role in SERS performance, we prepared a series of Cu scales by applying different Cu deposition time (DT) from 5 min to 25 min at an interval of 5 min. It was found that minimal time of 10 min for Cu plating was required to achieve continuous and self-supporting Cu scale replicas (**Figure 2**). A shorter DT of 5 min induced a discontinuous layer of deposited Cu NPs on the main ridges and ribs. Some tiny Cu structures might in turn collapse after the dissolving of the chitinous bio-templates (Figure 2b). In comparison, when a longer DT of 15 min was applied, coarsened Cu morphologies were obtained (Figure 2d) because of the excessively assembled Cu NPs. This phenomenon became more apparent if DT was prolonged to 20 min (Figure 2e). As Cu particles aggregated with further increase in DT (25 min), the microstructures of the Cu replica were filled by Cu NPs and the original scale morphologies could barely be maintained (Figure 2f). These results confirm that DT can be efficiently applied to control the morphologies of replicas through tuning the thickness of the deposited Cu layers on butterfly wing scales, providing us a series of samples to investigate the coupling effects between the structures and the SERS properties. Figure 2g shows the corresponding XRD results of Cu replicas prepared under different Cu plating time. Much more precise {111} peaks are shown separately in Figure 2h, which were collected at a low scan rate of 0.5° min^{-1}. The crystallite sizes were calculated to be 15.9 nm, 16.9 nm, 19.2 nm, 22.4 nm, and 28.6 nm, respectively, with an increase in DT, indicating that the crystallites grew up as the electroless deposition process lasted (Figure 2i).

2.2. Effects of Various Periodicities in Cu Scales on SERS Performance

We evaluated the SERS performance of these structure-tuned Cu scales. A setup for Raman measurements using 3D Cu

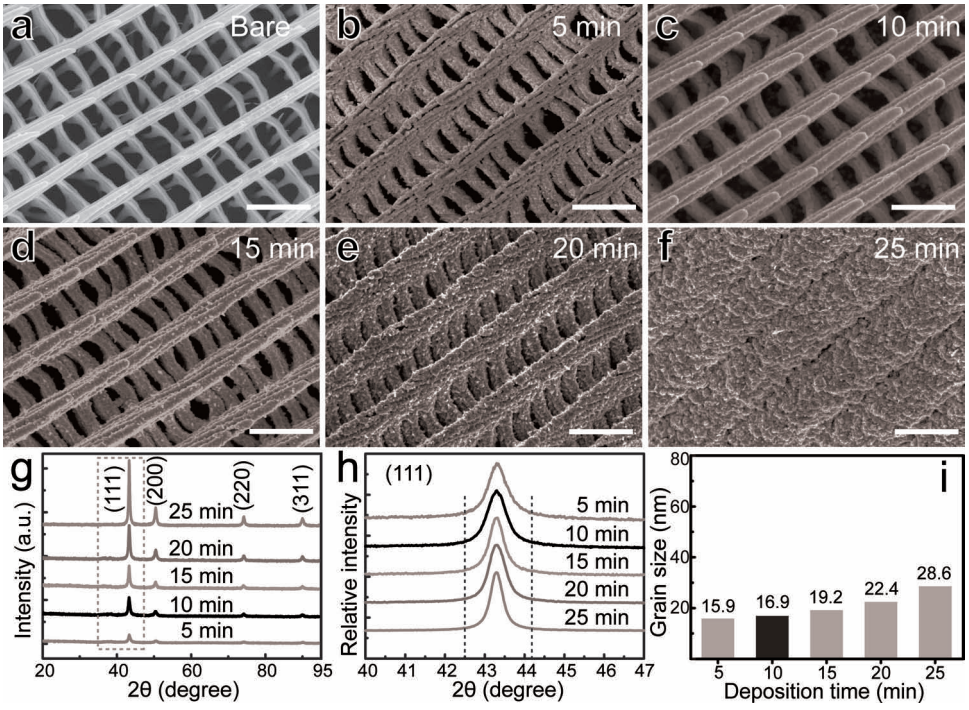

Figure 2. FESEM images and XRD results showing the influence from deposition time on the periodic structures of Cu scales. a) Chitin-based scale of *E. mulciber*. b)–f) Cu scales fabricated via electroless Cu deposition for b) 5 min, c) 10 min, d) 15 min, e) 20 min, and f) 25 min, respectively. Scale bars: 1 µm. g) XRD results of Cu scales prepared under different deposition time. h) XRD results at {111} peak (scan rate: 0.5° min^{-1}). The peak intensities of different samples were normalized to unity for comparison. i) Calculated crystallite size (Scherrer Formula) from h).

wing scales as SERS substrates is depicted in Scheme S1 in the Supporting Information, where we also present a comparison demonstrating the influence on SERS properties exerted by 3D sub-micrometer structures (Figure S2 and Figure S3, Supporting Information). Experimental results (Figure S3, Supporting Information) show that 10-min-deposited Cu substrates with exact scale morphologies (Figure 2c) generated Raman signals of rhodamine 6G (R6G) one order of magnitude stronger than their counterparts in similar Cu crystallite size (ca. 17 nm) but without 3D bio-morphologies, clearly exhibiting a structural effect.

Since there are at least three levels of periodicities in a scale structure, i.e. gaps between adjacent main ridges (referred to hereafter as P1), horizontal struts (P2), and ribs (P3), in order to gain a deep understanding of the origin of the observed structural effect, an estimation of the individual contributions from these structural units on SERS properties should be made. We applied R6G ethanol solution of 10^{-5} M as analyte to compare the SERS performance of the structures presented in Figure 2b–f. As shown in **Figure 3**, the Raman intensity started to increase with the Cu plating time, and reached its maximum at DT = 10 min. The integrated intensity of the R6G peak at 1650 cm^{-1} acquired on the 10-min-deposited sample (DT–10, Figure 2c) was ca. 3.5 times stronger (see Figure 3h) than that on DT–5 (Figure 2b). This phenomenon can be attributed to the inhomogeneous NP coating on the bio-template within a comparatively short DT. When DT increased over 10 min, the Raman intensity began to decline. The intensity reduced slightly as DT reached 15 min. However, if DT increased to 20 min, and 25 min further, the SERS intensity would significantly decrease. The integrated intensity of the 1650 cm^{-1} Raman band acquired on DT–10 was ca. 2.5 and 5 times of magnitude higher than those on DT–20 and DT–25, respectively (Figure 3h). It is worth mentioning that, as the "window" edges (Figure 2c) approached to each other (Figure 2f) with prolonged DT, periodicities in ribs (P3), struts (P2), and even main ridges (P1) were broken. Although the Cu grain size simultaneously increased as deposition lasted (Figure 2i), approaching to the reported optimal size of 50 nm for SERS on Cu,[30] it still could not compensate the loss of the localized EM fields contributed by the 3D morphologies (Figure 1c,d). These results also indicate that the significant Raman enhancement found in metallic butterfly scales originate predominantly from their 3D sub-micrometer structures rather than the morphological or size effects of the metal NPs themselves.[31]

By further analyzing the data from Figure S3 (Supporting Information) in the Supporting Information, we obtain two facts on the additional contributions from various periodicities (P1–P3) to Raman enhancement over structure-less individual NPs:

Under the same NP size (ca. 17 nm), perfectly structured scale replicas (DT–10) enhanced the Raman intensity ca. 10 times of magnitude higher than their as-ground counterparts with 3D structures drastically broken, suggesting that the whole enhancement contribution from P1+P2+P3 to SERS was about 10 times over individual NPs without long-range structures (see Figure S3, Supporting Information).

Under the same NP size (ca. 22 nm), DT–20 whose P3 was partially broken and P1, P2 were kept, amplified analyte signals ca. 2.7 times of magnitude stronger than as-ground samples with all periodicities almost destroyed. This result indicates that the enhancement contribution from P1+P2 was about 2.7 times of magnitude over the structure-less individual NPs.

Hence, we consider that scale replicas of *E. mulciber* with additional P3 besides P1+P2 can generate Raman signals of analyte ca. 4 times stronger than structures with only P1+P2. For DT–15 (Figure 3d), the periodicities of struts (P2) and main ridges (P1) were still well kept as compared with DT–10 (Figure 3c). However, the SERS properties had started to decrease with 5 min longer in Cu deposition time. This phenomenon indicates as well that a smaller period, which originated from even more fine structures than main ridges and struts, was responsible for the observed significant enhancement of Raman signals. Such experimental evidence drove us to further focus our studies on the rib-structures with a period of ca. 20 nm (Figure 1j) located on main ridges of Cu scale replicas.[32–34]

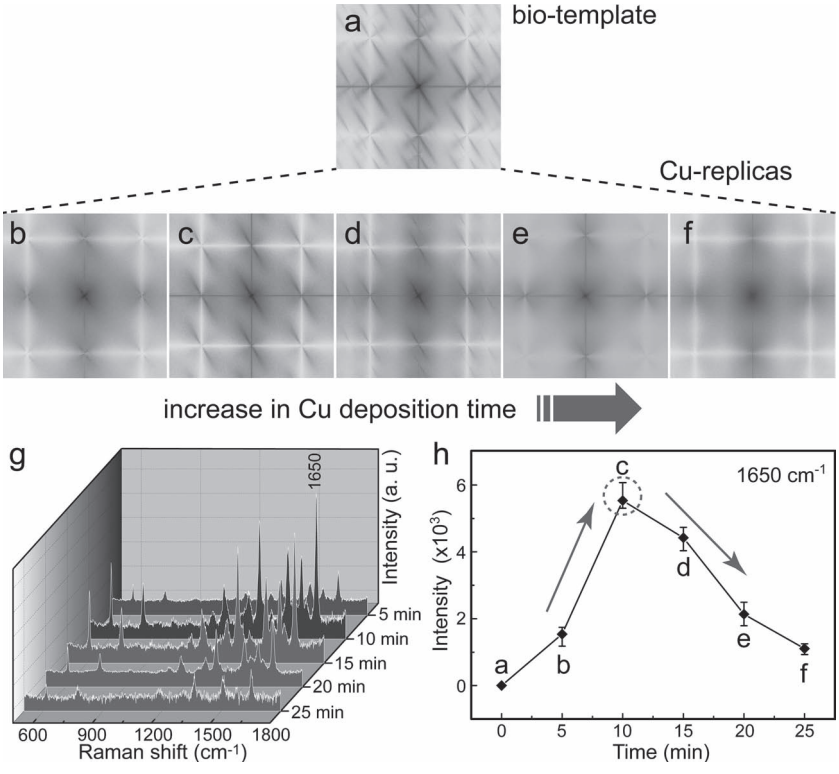

Figure 3. a–f) SEM images processed using fast fourier-transform from a) original scales and their replicas under Cu deposition time of b) 5 min, c) 10 min, d) 15 min, e) 20 min, and f) 25 min, respectively. g) SERS spectra of 10^{-5} M R6G collected on different Cu substrates corresponding to b–f). h) Raman intensities of (g) at 1650 cm^{-1}. There exists an optimal Cu deposition time of 10 min for the best SERS performance, corresponding to the morphology shown in Figure 2c.

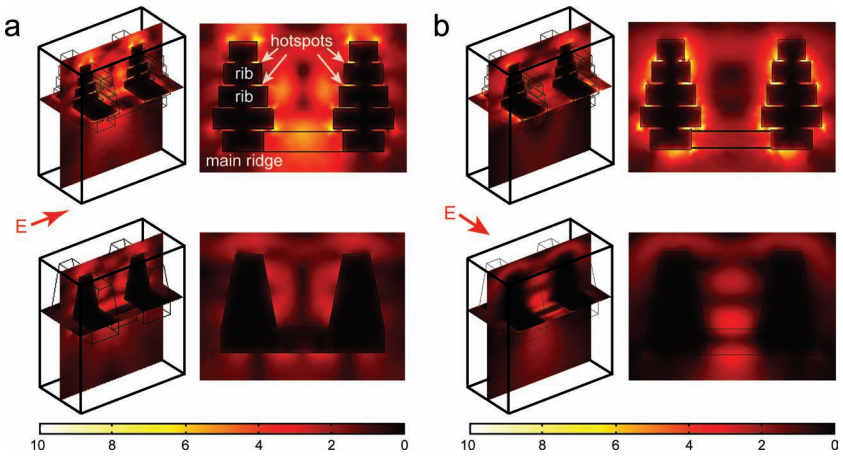

Figure 4. Distribution of EM fields excited by an incident light ($\lambda = 514.5$ nm) on Cu scales of *E. mulciber*. The incidence polarizations are a) perpendicular and b) parallel to the length direction of main ridges, respectively. Piled-up hotspots where EM fields are substantially enhanced can be identified in the models with rib-structures, which can amplify the Raman signals according to the electromagnetic theory of SERS. The scale bars denote the relative intensities of the excited EM fields against the incident EM field.

2.3. Simulation of the Hotspots Aroused by the Rib-Structures of Cu Scales

We studied the localized surface plasmon resonances using a finite element method (FEM, **Figure 4**). Detailed descriptions of the adopted models for calculation are provided in Figure S4 and Table S1 (Supporting Information), respectively, based on the data acquired from SEM observations. Figure 4a presents the calculated EM field distribution with the polarization (*E*-vector) of an incident radiation (514.5 nm) perpendicular to the length direction of main ridges. The Cu scale with rib-structures (10-min-deposited) exhibited "piled-up" hotspots along the normal of the scale surface. In comparison, these hotspots disappeared in the structure whose rib-gaps were filled with Cu as DT for Cu increased to 20 min. Similar phenomenon could be identified when the polarization was parallel to the length direction of main ridges (Figure 4b). It should be noted that our simulation did not consider the roughness of the Cu replica surface. A real situation should be between these two cases as the scattering of the originally polarized EM wave by the rough surfaces of Cu NPs could break the polarization. Since the SERS enhancement is approximately proportional to the fourth power of the EM field intensity according to the electromagnetic theory of SERS,[35–37] the simulation results suggest that the 3D Cu scales with fine rib-structures efficiently generated localized surface plasmons and substantially enhanced EM fields in the rib-gaps, providing hotspots especially arranged along the third direction vertical to the scale (substrate) surface. Such phenomenon can actually be found in models with rib-gaps of 20–50 nm, which will be published in details elsewhere.

2.4. SERS Performance of Cu Scales with Other Morphologies

We have checked this hypothesis in several other Cu scales with various morphologies, including those collected as bio-templates from the ventral forewing surface (referred to hereafter as B) and dorsal hindwing surface (C) of *E. mulciber*, the dorsal forewing surface of *Kallima inachus* (D), and the dorsal forewing surface of *Thaumantis diores* (E). Their morphologies, together with that of the Cu scale replicated from *E. mulciber*'s dorsal forewing (referred to hereafter as A) that have been discussed previously, are shown in **Figure 5** and **Figure 6**. Detailed dimensions of these replicas are generalized in **Table 1**. These scales have similar "window" structures but with different stacking modes and stacking numbers of ribs (SNR). As shown in Figure 6, the stacking modes of ribs are 4–3, 3–2, 3–2, 2, and 1 in SNR for A–E, respectively. Among all these samples, A has the largest SNR (4 ~ 3), which could favorably provide the most hotspots as discussed above and in turn yield the highest Raman enhancement (**Figure 7**). Meanwhile, the rib-gap gets narrower with the increase in SNR under the similar main-ridge-height for A–E (ca. 800 nm), which might also be responsible for the pronounced Raman signals acquired on A.[32,33] In comparison, B and C share the same stacking mode of ribs (3–2), and the

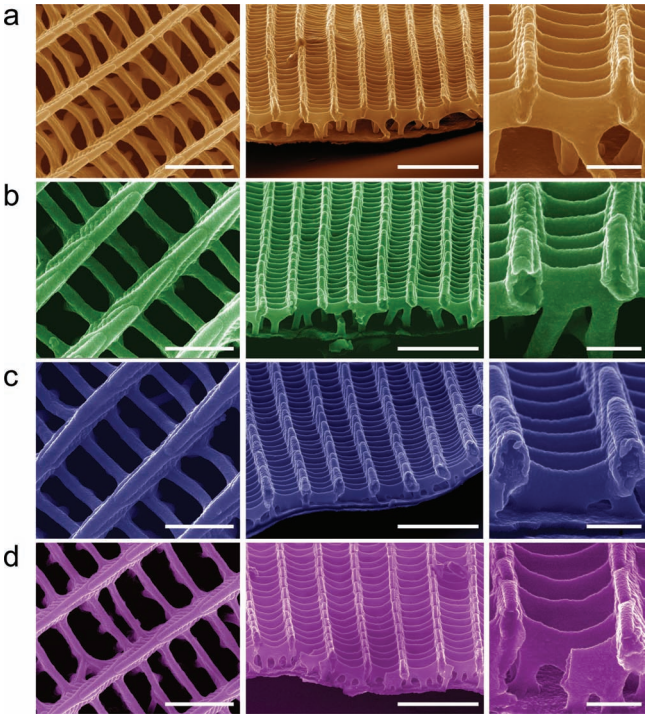

Figure 5. Cu replicas with topologically similar morphologies inherited from natural scales on a) ventral forewing surface of *E. mulciber* (referred to as B in the main text), b) dorsal hindwing surface of *E. mulciber* (C), c) dorsal forewing surface of *K. inachus* (D), and d) dorsal forewing surface of *T. diores* (E). The Cu deposition time was 10 min for these samples. Scale bars: 2 µm (left column), 5 µm (middle column), and 1 µm (right column).

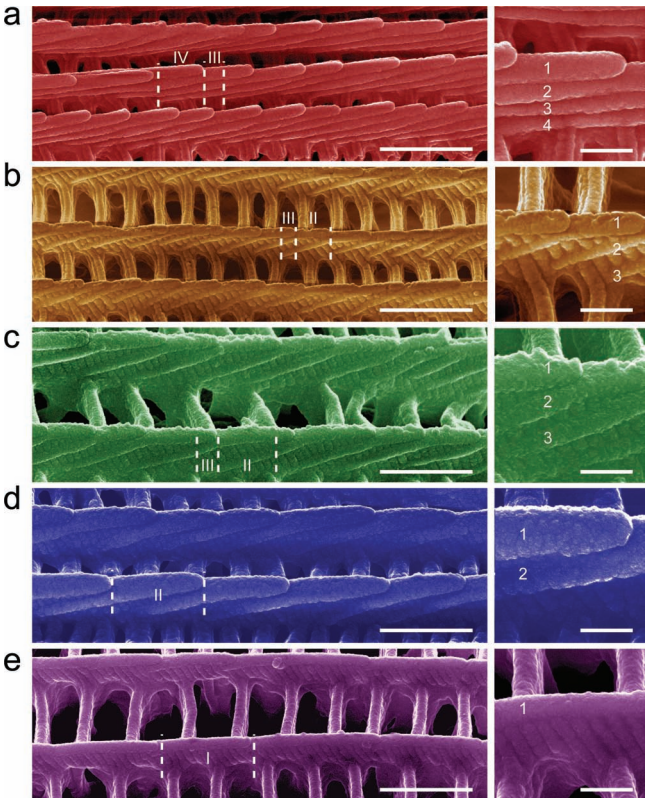

Figure 6. Rib-structures in Cu replicas converted from natural scales on a) dorsal forewing surface, b) ventral forewing surface, and c) dorsal hindwing surface of *E. mulciber*; d) dorsal forewing surface of *K. inachus*; e) dorsal forewing surface of *T. diores*. a)–e) correspond to scale A–E as mentioned in the main text, respectively. Stacking modes and numbers of ribs are marked herein. Scale bars: 2 μm (left column), 500 nm (right column).

distance between the main ridges of B (ca. 1.5 μm) is smaller than that of C (ca. 1.8 μm). Such morphologies make B and C exhibit lower ability in increasing Raman signals of analytes than A, and the enhanced R6G signals were weaker on C than on B as the density of hotspots in C is lower than that in B in a given area (Figure 7). Scales with further less SNR are shown in Figure 6d,e, respectively. SNR of D (2) is smaller than that of C (2 ~ 3), and the size of main-ridge-gap is larger in D than in C, giving rise to a lower hotspot density and consequently lower Raman enhancement ability for D. As SNR further decreases to

Table 1. Dimension list of the Cu scales presented in Figure 5.

Scale	Window Length [μm][a)]	Window Width [nm][a)]	Ridge Width [nm][a)]
A	0.68	320	200
B	1.52	500	200
C	1.80	780	285
D	2.00	650	300
E	2.12	695	220

[a)]Definitions of these dimensions can be found in Figure 1c. Data were averaged from at least ten positions.

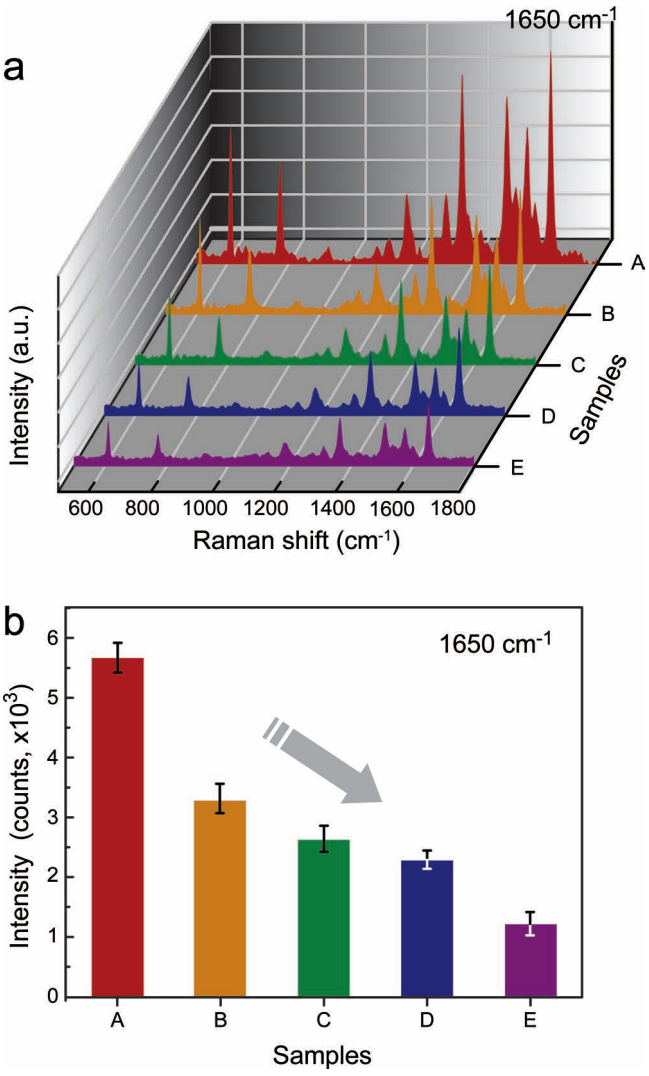

Figure 7. a) Raman spectra of R6G molecules absorbed on Cu scales described in Figure 5 and Figure 6 as SERS substrates. b) Comparison of Raman intensities at 1650 cm^{-1}.

1, E gave the lowest Raman signals. These experimental results are consistent with our hypothesis presented in the previous section.

As we have demonstrated, although *Lepidopterans* initially developed those light-responsive hierarchical structures for propagation and camouflage, etc.,[26–29,38,39] they could still offer other light concerned functions aroused by the development of state-of-the-art science and technology.[40,41] Based on recently developed ideas, e.g., the "nano-antenna",[18] several high-quality artificial superstructures including nanorod assemblies,[17] nano-canal arrays,[19] and petal-like arrayed structures,[20] etc., have been successfully fabricated to arrange the hotspots out of the substrate plane. However, the morphological varieties of these materials would be somewhat limited as compared with those of the metallic replicas of the nature-designed butterfly scales. Human beings have actually been farming some species of *Lepidopterans* for thousands of years. For example, the caterpillars of *Bombyx mori* (silkworm) gives

us excellent silk products. Considering many adult *Lepidopterans* have a short life cycle (in weeks), we can use their wing scales as bio-templates for replication after their natural death. We have also evaluated the SERS properties of a whole Cu wing of *E. mulciber* without removing the original chitin-based structures (Figure S5, Supporting Information), which can be synthesized within thirteen hours in an ordinary laboratory. The lowest detection limit in either R6G or crystal violet (i.e. CV, another widely used analyte for SERS study) concentration is as low as 10^{-8} M. Thus, Cu SERS substrates with optimized 3D periodic structures inherited from butterfly wing scales are mass-producible consumables for sensitive molecule-detection by virtue of their high ability in Raman signal enhancement, and especially, the ultra low cost as compared with their Au and Ag counterparts for certain applications.[42–44]

3. Conclusions

We have demonstrated the influence on the SERS properties exerted by the rib-structures in Cu butterfly wing scales. The pronounced Raman enhancement mainly originates from the 3D sub-micrometer periodic rib-structures located on the main ridges of Cu scales rather than the morphological or size effects of Cu NPs themselves. Similar to the more floors a building has, the more residents it can contain, more periodically arranged rib-layers per unit square result in more piled-up hotspots, leading to better SERS performance. It is still quite difficult to efficiently generate reproducible and mass-producible 3D sub-micrometer structures for SERS applications, but nature has already engineered lots of such candidates via millions of years' selection. By further introducing the presently well-developed tuning methods to these nature-designed 3D scaffolds, e.g., the control of NP morphologies or the formation of core-shell NP structures with multi-components,[45–47] even higher SERS properties can be expected. This work paves the way to the optimal s cale candidates out of ca. 175 000 *Lepidopteran* species as bio-templates to replicate for SERS applications, and thus helps bring affordable SERS substrates as consumables with high sensitivity, high reproducibility, and low cost to ordinary laboratories across the world.

4. Experimental Section

Materials: We chose wing scales from *E. mulciber, K. inachus*, and *T. diores* as original bio-templates to replicate. These scales were first covered by Au NPs, which served as catalysts for the subsequent continuous deposition of Cu. The original chitin-based textures were finally removed by exposure to H_3PO_4. A general synthesis route can be found in the literature.[21] We herein set the plating time of Cu from 5 min to 25 min at an interval of 5 min to study the effects of various sub-micrometer structures on the induced SERS properties.

Microstructural Characterization: The synthesized samples were examined using XRD on a D-max/2550 X-ray diffractometer system (Rigaku, 35 kV, 20 mA, $Cu_{K\alpha}$), operated at a scan rate of 4° min^{-1} and a step size of 0.05° in 2θ. FESEM observation was conducted on an FEI Quanta FEG 250 (20 kV). TEM images were recorded on an FEI Tecnai 20 (200 kV). Optical microscope observation was carried out using a VHX-1000 stereomicroscope from Keyence.

Measurement of Raman Spectra: Raman scattering spectra were acquired using a Renishaw inVia Raman microscope operated with a 514.5 nm Ar ion laser (beam size: ca. 2 μm, using a 50× short focal length objective). An irradiation power of approximately 2 mW (10% of the laser power) was used to excite the samples. The integration time was 20 s. R6G and CV were respectively dissolved into ethyl alcohol to form solutions with various concentrations for detection. The Cu butterfly wing scales as substrates were immersed in the corresponding solutions for 2 h towards a sufficient molecule adsorption before SERS measurements. All the Raman signals were acquired at least for ten times from different spots on various Cu scale replicas.

Modeling and Simulation: A finite element method (FEM) realized by commercial software (COMSOL 3.5a) was adopted to simulate the distribution of electromagnetic fields in a three dimensional space. We only computed the EM field distribution caused by the long-range smooth structures, and ignored the roughness of the metal surface. The models and detailed structural dimensions of two different substrates are shown in Figure S4 and Table S1 in the Supporting Information. The dielectric constant of air was 1 and the dielectric constant of Cu was obtained from the literature.[48] An incident plane electromagnetic wave (514.5 nm) was set to propagate against the normal of the scale surface with polarization (*E*-vector) in the mentioned directions. In the calculations, initial amplitude of EM field was set to be 1.

Supporting Information

Supporting Information is available from the Wiley Online Library or from the author.

Acknowledgements

This work was supported by the National Natural Science Foundation of China (Grant No. 51131004 and 51171110), the National Basic Research Program of China (973 Program, Grant No. 2012CB619600), the Shanghai Science and Technology Committee (Grant No. 10JC1407600), and the Cultivation Fund for Excellent Doctoral Thesis of Shanghai Jiao Tong University. L.X. and X.Z. appreciate the financial support from the Third Shanghai Innovation Experiment Program for Undergraduate Students and the Participation in Research Program (PRP) of Shanghai Jiao Tong University. We thank Prof. Won-Jin Moon, Dr. Deok-Min Song, and Ms. Ye-Bin Kwon at Gwangju Center, Korea Basic Science Institute, for TEM observations.

Received: December 5, 2011
Revised: December 21, 2011
Published online: February 13, 2012

[1] D. K. Lim, K. S. Jeon, H. M. Kim, J. M. Nam, Y. D. Suh, *Nat. Mater.* **2010**, *9*, 60.
[2] R. M. Jarvis, R. Goodacre, *Chem. Soc. Rev.* **2008**, *37*, 931.
[3] J. P. Camden, J. A. Dieringer, J. Zhao, R. P. Van Duyne, *Acc. Chem. Res.* **2008**, *41*, 1653.
[4] A. Matschulat, D. Drescher, J. Kneipp, *ACS Nano* **2010**, *4*, 3259.
[5] N. Guarrotxena, B. Liu, L. Fabris, G. C. Bazan, *Adv. Mater.* **2010**, *22*, 4954.
[6] L. L. Yang, B. Yan, W. R. Premasiri, L. D. Ziegler, L. Dal Negro, B. M. Reinhard, *Adv. Funct. Mater.* **2010**, *20*, 2619.
[7] S. Keren, C. Zavaleta, Z. Cheng, A. de la Zerda, O. Gheysens, S. S. Gambhir, *Proc. Natl. Acad. Sci. USA.* **2008**, *105*, 5844.
[8] J. Kneipp, H. Kneipp, A. Rajadurai, R. W. Redmond, K. Kneipp, *J. Raman. Spectrosc.* **2009**, *40*, 1.
[9] N. R. Jana, T. Pal, *Adv. Mater.* **2007**, *19*, 1761.
[10] M. J. Mulvihill, X. Y. Ling, J. Henzie, P. D. Yang, *J. Am. Chem. Soc.* **2010**, *132*, 268.

[11] W. Wang, Z. P. Li, B. H. Gu, Z. Y. Zhang, H. X. Xu, *ACS Nano* **2009**, *3*, 3493.
[12] L. H. Lu, G. Y. Sun, H. J. Zhang, H. S. Wang, S. Q. Xi, J. Q. Hu, Z. Q. Tian, R. Chen, *J. Mater. Chem.* **2004**, *14*, 1005.
[13] N. A. Abu Hatab, J. M. Oran, M. J. Sepaniak, *ACS Nano* **2008**, *2*, 377.
[14] Q. Yu, P. Guan, D. Qin, G. Golden, P. M. Wallace, *Nano Lett.* **2008**, *8*, 1923.
[15] M. L. Jin, V. Pully, C. Otto, A. van denBerg, E. T. Carlen, *J. Phys. Chem. C* **2010**, *114*, 21953.
[16] K. B. Crozier, W. Q. Zhu, M. G. Banaee, D. X. Wang, Y. Z. Chu, *Small* **2011**, *7*, 1761.
[17] R. A. Alvarez-Puebla, A. Agarwal, P. Manna, B. P. Khanal, P. Aldeanueva-Potel, E. Carbó-Argibay, N. Pazos-Pérez, L. Vigderman, E. R. Zubarev, N. A. Kotov, L. M. Liz-Marzán, *Proc. Natl. Acad. Sci. USA* **2011**, *108*, 8157.
[18] G. W. Bryant, F. J. García de Abajo, J. Aizpurua, *Nano Lett.* **2008**, *8*, 631.
[19] H. Ko, S. Singamaneni, V. V. Tsukruk, *Small* **2008**, *4*, 1576.
[20] C. Qian, C. Ni, W. X. Yu, W. G. Wu, H. Y. Mao, Y. F. Wang, J. Xu, *Small* **2011**, *7*, 1801.
[21] Y. W. Tan, J.-J. Gu, X. N. Zang, W. Xu, K. C. Shi, L. H. Xu, D. Zhang, *Angew. Chem. Int. Ed.* **2011**, *50*, 8307.
[22] N. L. Garrett, P. Vukusic, F. Ogrin, E. Sirotkin, C. P. Winlove, J. Moger, *J. Biophotonics* **2009**, *2*, 157.
[23] Y. W. Tan, X. N. Zang, J.-J. Gu, D. X. Liu, S. M. Zhu, H. L. Su, C. L. Feng, Q. L. Liu, W. M. Lau, W. J. Moon, D. Zhang, *Langmuir* **2011**, *27*, 11742.
[24] J. Han, H. L. Su, D. Zhang, J. J. Chen, Z. X. Chen, *J. Mater. Chem.* **2009**, *19*, 8741.
[25] P. Vukusic, J. R. Sambles, C. R. Lawrence, R. J. Wootton, *Proc. R. Soc. B* **1999**, *266*, 1403.
[26] Y. Obara, T. Hidaka, *Proc. Jpn. Acad.* **1968**, *44*, 828.
[27] A. Sweeney, C. Jiggins, S. Johnsen, *Nature* **2003**, *423*, 31.
[28] N. I. Morehouse, P. Vukusic, R. Rutowski, *Proc. R. Soc. B* **2007**, *274*, 359.
[29] M. Joron, L. Frezal, R. T. Jones, N. L. Chamberlain, S. F. Lee, C. R. Haag, A. Whibley, M. Becuwe, S. W. Baxter, L. Ferguson, *Nature* **2011**, *477*, 203.
[30] Y. Mo, I. Mörke, P. T. Wachter, *Solid State Commun.* **1984**, *50*, 829.
[31] P. Tessier, O. D. Velev, A. T. Kalambur, A. M. Lenhoff, J. F. Rabolt, E. W. Kaler, *Adv. Mater.* **2001**, *13*, 396.
[32] S. Z. Li, M. L. Pedano, S. H. Chang, C. A. Mirkin, G. C. Schatz, *Nano Lett.* **2010**, *10*, 1722.
[33] X. G. Deng, G. B. Braun, S. Liu, P. F. Sciortino, B. Koefer, T. Tombler, M. Moskovits, *Nano Lett.* **2010**, *10*, 1780.
[34] V. Liberman, C. Yilmaz, T. M. Bloomstein, S. Somu, Y. Echegoyen, A. Busnaina, S. G. Cann, K. E. Krohn, M. F. Marchant, M. Rothschild, *Adv. Mater.* **2010**, *22*, 4298.
[35] H. Im, K. C. Bantz, N. C. Lindquist, C. L. Haynes, S. H. Oh, *Nano Lett.* **2010**, *10*, 2231.
[36] N. J. Halas, S. Lal, W. Chang, S. Link, P. Nordlander, *Chem. Rev.* **2011**, *111*, 3913.
[37] J. D. Caldwell, O. Glembocki, F. J. Bezares, N. D. Bassim, R. W. Rendell, M. Feygelson, M. Ukaegbu, R. Kasica, L. Shirey, C. Hosten, *ACS Nano* **2011**, *5*, 4046.
[38] A. R. Parker, *J. Opt. A-Pure. Appl. Opt.* **2000**, *2*, R15.
[39] P. Vukusic, J. R. Sambles, *Nature* **2003**, *424*, 852.
[40] C. Aguirre, E. Reguera, A. Stein, *Adv. Funct. Mater.* **2010**, *20*, 2565.
[41] M. R. Jorgensen, M. H. Bartl, *J. Mater. Chem.* **2011**, *21*, 10583.
[42] M. Zamuner, D. Talaga, F. Deiss, V. Guieu, A. Kuhn, P. Ugo, N. Sojic, *Adv. Funct. Mater.* **2009**, *19*, 3129.
[43] Q. M. Yu, S. Braswell, B. Christin, J. J. Xu, P. M. Wallace, H. Gong, D. Kaminsky, *Nanotechnology* **2010**, *21*, 355301.
[44] E. S. Shibu, K. Kimura, T. Pradeep, *Chem. Mater.* **2009**, *21*, 3773.
[45] L. Lu, A. Eychmuller, *Acc. Chem. Res.* **2008**, *41*, 244.
[46] R. Gunawidjaja, E. Kharlampieva, I. Choi, V. V. Tsukruk, *Small* **2009**, *5*, 2460.
[47] J.-J. Feng, U. Gernert, P. Hildebrandt, I. M. Weidinger, *Adv. Funct. Mater.* **2010**, *20*, 1954.
[48] S. G. Rodrigo, F. J. García-Vidal, L. Martín-Moreno, *Phys. Rev. B* **2008**, *77*, 075401.